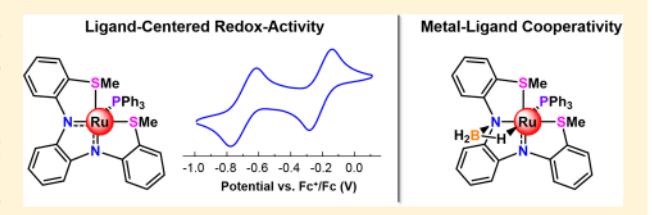
Ru(II) Complexes with a Chemical and Redox-Active S₂N₂ Ligand: Structures, Electrochemistry, and Metal-Ligand Cooperativity

Gummadi Durgaprasad, Javier A. Luna, Kyle D. Spielvogel, Christian Haas, Scott K. Shaw,*® and Scott R. Daly*®

Department of Chemistry, The University of Iowa, E331 Chemistry Building, Iowa City, Iowa 52242-1294, United States

Supporting Information

ABSTRACT: Here we describe the synthesis, structures, and reactivity of Ru complexes containing a triaryl, redox-active S2N2 ligand derived from o-phenylenediamine and thioanisole subunits. The coordination chemistry of N_iN' -bis[2-(methylthio)phenyl]-1,2-diaminobenzene [$H_2(^{Me}SNNS^{Me})$] was established by treating $RuCl_2(PPh_3)_3$ with $H_2(^{Me}SNNS^{Me})$ to yield { $Ru[H_2(^{Me}SNNS^{Me})]$ - $Cl(PPh_3)$ }Cl (1). Coordinated $H_2(^{Me}SNNS^{Me})$ was sequentially deprotonated to form $Ru[H(^{Me}SNNS^{Me})]$ Cl(PPh_3) (2) followed



by the five-coordinate, square pyramidal complex Ru(MeSNNSMe)(PPh3) (3). Single-crystal X-ray diffraction (XRD) studies revealed that the ligand structurally rearranged around the metal at each deprotonation step to conjugate the adjacent aryl groups with the o-phenylenediamine backbone. Deprotonation of 2 with NaBH₄ or treatment of 3 with BH₃ tetrahydrofuran (THF) yielded Ru[(µ-H)BH₂](MeSNNSMe)(PPh₃) (5) with BH₃ bound across a Ru-N bond in a metal-ligand cooperative fashion. The cyclic voltammogram of 3 in THF revealed three redox events consistent with one-electron oxidations and reductions of the o-phenylenediamine backbone and the metal (Ru³⁺/Ru²⁺). Reactions of 3 with CO, HBF₄, and benzoic acid yielded the new complexes Ru(MeSNNSMe)(CO)(PPh₃), {Ru[H(MeSNNSMe)](PPh₃)(THF)}BF₄, and Ru[H(MeSNNSMe)](PPh₃)(PhCO₂), indicating broader suitability for small molecule binding and reactivity studies. Subsequent nuclear magnetic resonance spectroscopy, infrared spectroscopy, and mass spectrometry data are reported in addition to molecular structures obtained from single-crystal XRD studies.

INTRODUCTION

Redox-active ligands continue to garner significant interest because of their ability to mediate multielectron redox processes deemed inaccessible with metals alone. 1-3 For example, base metals with limited redox activity (e.g., Zr and Al),4,5 as well as first-row transition metals and actinides that prefer one-electron redox processes, ^{6,7} have been combined with redox-active ligands to achieve two-electron oxidative addition and reductive elimination reactions more typical of second- and third-row transition metals. These efforts reveal significant potential for expanding the scope of earth-abundant metals in homogeneous catalysis and present opportunities for new multielectron small molecule transformations with precious and nonprecious metals.

o-Phenylenediamine and derivatives thereof are archetypal redox-active ligands capable of undergoing two successive oneelectron oxidations when bound to a wide variety of metals.8-22 Fully reduced o-phenylenediamine can be oxidized by one electron to form the o-diiminosemiquinone radical and then oxidized again to form the fully oxidized o-diiminoquinone (Chart 1). It has been shown that this redox activity can be altered by flanking o-phenylenediamine with supporting aryl groups, especially those containing electron donor substituents that bind to the metal and conjugate flanking aryl groups. For example, it was reported by Thomas and co-workers that tetradentate o-phenylenediamine ligands containing supporting

Chart 1. o-Phenylenediamine Redox Transformations and Comparison of Triaryl Tetradentate Ligands with o-Phenylenediamine Subunits

aniline groups yield redox activity localized on the flanking aryl groups instead of the backbone.²³ In contrast, isostructural ONNO complexes, which contain phenol arms instead of aniline, exhibit redox activity both at the o-phenylenediamine and on the flanking phenolate groups.^{4,24–26} Ligands in both examples contain N-H (aniline) or O-H (phenol) sub-

Received: August 14, 2017 Published: October 11, 2017

Scheme 1. Synthesis of H₂(MeSNNSMe) and {Ru[H₂(MeSNNSMe)]Cl(PPh₃)}Cl (1)

stituents on the flanking arms that can (1) be deprotonated and (2) participate in ligand redox transformations via formation of C=NH and C=O bonds, respectively. We postulated that replacing the NH and OH groups with non-acidic neutral donors such as thioethers would provide a means to direct the redox reactivity exclusively to the o-phenylenediamine backbone. This hypothesis was inspired by recent reports by Goswami and co-workers that bidentate aminothiophenols (-SH) and aminothioethers (-SR) exhibit divergent redox reactivity when bound to Ru.²⁷ Replacing the S-H protons with methyl groups shuts down the participation of sulfur in redox events.

To test our hypothesis, we prepared an o-phenylenediamine-derived S_2N_2 ligand with thioanisole groups [abbreviated as $H_2(^{\text{Me}}SNNS^{\text{Me}})$ (Chart 1)] and examined its coordination chemistry and reactivity with Ru(II). Ru compounds containing tetradentate ligands are known to be highly active catalysts for a variety of transformations, 28,29 and our long-term goal is to combine this exceptional reactivity with redox-active ligands to promote new, electrochemically mediated small molecule transformations. As we show here, redox-active $H_2(^{\text{Me}}SNNS^{\text{Me}})$ yields Ru complexes that undergo sequential N deprotonation to yield diverse structures that depend on the number of protonated N atoms and the field strength of ancillary ligands such as CO. Moreover, we report that the deprotonated N atoms are sufficiently nucleophilic to participate in metalligand cooperative (MLC) binding, 30 a type of substrate binding that is relevant to CO_2 activation. $^{31-36}$

RESULTS AND DISCUSSION

Synthesis and Ru(II) Coordination Chemistry. H₂(MeSNNSMe) was prepared by Buchwald-Hartwig crosscoupling of 2 equiv of 2-bromothioanisole with o-phenylenediamine in toluene with excess NaOtBu and catalytic amounts of Pd₂(dba)₃ and rac-BINAP. The ligand was isolated by extraction with toluene and purification by silica-gel column chromatography in 74% yield. ¹H and ¹³C nuclear magnetic resonance (NMR) spectroscopy, microanalysis, mass spectrometry, and single-crystal X-ray diffraction (XRD) confirmed the identity of H₂(MeSNNSMe) (Figure S1). The chemically equivalent SMe resonances appeared as singlets in the ¹H and ^{13}C NMR spectra in CDCl₃ at δ 2.28 and 17.96, respectively. The N-H proton signal was observed as a broad resonance at δ 6.68 in the ${}^{\rm I}{\rm H}$ NMR spectrum. The remaining NMR peak positions and integrations support the chelating triaryl framework.

Access to the desired Ru(II) coordination chemistry was established by refluxing a 1:1 mixture of $H_2(^{Me}SNNS^{Me})$ and RuCl₂(PPh₃)₃ in tetrahydrofuran (THF) overnight. The yellow precipitate that formed was recrystallized from dichloromethane and pentane to yield pale-yellow crystals of {Ru-[H₂($^{Me}SNNS^{Me}$)]Cl(PPh₃)}Cl (1) (Scheme 1). Single-crystal

XRD studies revealed that 1 has an octahedral coordination geometry with $H_2(^{Me}SNNS^{Me})$ arranged in a *cis-\alpha* configuration, and PPh₃ and chloride occupy the remaining coordination sites (Figure 1). The remaining positive charge

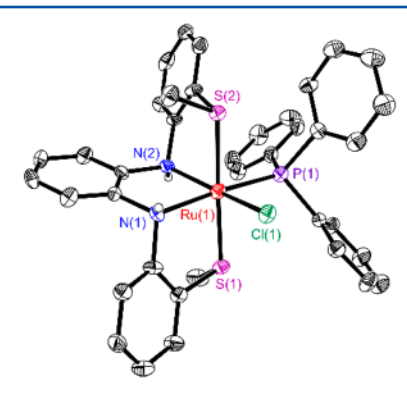


Figure 1. Molecular structure of 1. Ellipsoids are drawn at the 35% probability level. The outer-sphere chloride and hydrogen atoms (except those attached to N) have been omitted.

on the complex ion was balanced by an outer-sphere chloride that hydrogen bonds to one of the N–H groups. Selected bond distances and angles are listed in Table 1. The *trans* Ru–S distances of 2.321(2) and 2.345(2) Å are identical to those reported for *trans* thioanisole groups in Ru complexes containing pentadentate pyN₂H₂S₂² ligands³⁷ and slightly shorter than Ru–SMe distances reported by Dub and Gordon for a (NNS)RuCl₂(PPh₃) complex at 2.310(2) Å ³⁸ The *trans* Ru–P and Ru–N distances of 2.333(2) and 2.173(5) Å, respectively, are slightly shorter than those reported previously [2.356(2) and 2.205(5) Å, respectively] for a Ru triphenyl-phosphine complex with a pentadentate N₂S₃ ligand.³⁹

The 1 H NMR spectrum of 1 collected in DMSO- d_6 revealed two SMe resonances at δ 2.04 and 2.36 and two broad N–H resonances at δ 7.92 and 9.71, as expected on the basis of their chemical inequivalency. The remaining peaks in the aryl region were consistent with the presence of phenyl protons on PPh₃ and the $H_2(^{\text{Me}}\text{SNNS}^{\text{Me}})$ ligand. A single peak in the ^{31}P NMR spectrum at δ 44.5 confirmed the presence of bound PPh₃.

We next explored the acid/base chemistry of coordinated $H_2(^{Me}SNNS^{Me})$. Addition of 1 equiv of NEt₃ to a 1:1 mixture of RuCl₂(PPh₃)₃ and $H_2(^{Me}SNNS^{Me})$ in benzene resulted in dehydrohalogenation and formation of the monoprotonated complex Ru[H($^{Me}SNNS^{Me}$)]Cl(PPh₃) (2) (Scheme 2). Several stereoisomers of 2 are possible (*vide infra*), and indeed, two diastereomers are observed in the ¹H NMR spectrum. At room temperature, two sets of broad SMe ¹H resonances were observed in CD₂Cl₂ at δ 1.79 and 2.02 (2) and at δ 1.58 and 2.42 (2') in a 1.7:1 ratio. Cooling the solution to -80 °C sharpened the ¹H NMR resonances so that we could more

Table 1. Selected Bond Distances and Angles from Single-Crystal X-ray Diffraction Data of 1-8

	1	2a	2b			4	S	9	7	∞	
	$L = Cl^{-}$	$L = Cl^{-}$	L = Cl ⁻	ю	•	L = MeCN	T = H	T = CO	L = THF	$L = O_2($	CPh-
Ru-N	2.143(5)	2.070(2)	2.076(2)	2.006(6)	2.008(6)	2.034(3)	2.039(4)	2.062(5)	2.065(4)	2.082(4)	2.059(5)
	2.173(5)	2.133(2)	2.139(1)	2.017(5)	2.009(6)	2.046(4)	2.097(4)	2.077(6)	2.159(5)	2.145(4)	2.140(4)
Ru-S	2.321(2)	2.2908(8)	2.2940(5)	2.330(2)	2.329(2)	2.330(1)	2.327(1)	2.354(2)	2.274(2)	2.275(2)	2.289(2)
	2.345(2)	2.3007(8)	2.3032(6)	2.338(2)	2.322(2)	2.323(1)	2.316(1)	2.432(2)	2.303(2)	2.322(2)	2.327(1)
Ru-P	2.333(2)	2.3219(7)	2.3415(6)	2.214(2)	2.196(2)	2.272(1)	2.317(1)	2.333(2)	2.340(2)	2.338(2)	2.329(2)
Ru-L	2.420(2)	2.4236(8)	2.4303(6)	I	ı	2.136(3)	1.77(4)	1.863(7)	2.205(4)	2.117(4)	2.120(4)
N-C	1.495(9)	1.366(3)	1.377(2)	1.39(1)	1.39(1)	1.378(5)	1.385(5)	1.38(1)	1.367(7)	1.334(7)	1.364(7)
	1.492(8)	1.385(3)	1.380(2)	1.39(1)	1.39(1)	1.378(6)	1.374(6)	1.39(1)	1.391(8)	1.392(7)	1.392(7)
	1.485(8)	1.462(3)	1.466(2)	1.39(1)	1.39(1)	1.390(6)	1.465(6)	1.39(1)	1.471(8)	1.477(7)	1.473(8)
	1.472(9)	1.492(3)	1.491(2)	1.40(1)	1.41(1)	1.391(7)	1.452(6)	1.42(1)	1.486(7)	1.500(7)	1.484(8)
N-Ru-N	82.7(2)	81.46(8)	81.61(6)	79.8(2)	80.0(2)	80.9(1)	80.2(1)	79.3(2)	79.1(2)	80.4(2)	79.8(2)
S-Ru-S	175.67(7)	97.11(2)	98.75(2)	107.84(8)	107.73(8)	109.49(4)	110.23(4)	97.37(7)	88.54(6)	92.72(6)	93.67(6)
N-Ru-S	82.5(2)	83.92(6)	83.61(4)	84.1(2)	84.2(2)	84.6(1)	83.9(1)	79.3(2)	83.6(1)	82.8(1)	82.4(1)
	84.3(1)	84.31(6)	84.34(4)	84.1(2)	84.6(2)	84.7(1)	85.5(1)	83.8(2)	85.3(1)	84.3(1)	85.2(1)
	94.9(1)	91.12(6)	90.05(4)	159.1(2)	160.1(2)	164.6(1)	158.5(1)	91.8(2)	92.9(1)	93.6(1)	92.4(1)
	101.6(2)	165.75(6)	165.75(4)	159.3(2)	160.3(2)	165.1(1)	165.7(1)	162.6(2)	161.2(1)	162.7(1)	162.1(1)
N-Ru-P	99.5(2)	96.26(6)	102.02(4)	103.2(2)	102.2(2)	93.3(1)	95.5(1)	91.7(2)	98.9(1)	102.6(1)	96.9(1)
	175.9(2)	174.65(6)	176.08(5)	104.9(2)	103.6(2)	93.4(1)	104.6(1)	91.7(2)	177.0(1)	176.9(1)	176.4(1)
S-Ru-P	88.85(6)	93.47(3)	91.84(2)	91.75(8)	91.50(8)	90.72(4)	87.08(4)	92.73(7)	89.20(6)	87.22(6)	88.82(6)
	91.82(7)	97.86(3)	91.97(2)	93.51(8)	93.35(8)	92.58(4)	91.17(4)	169.61(7)	98.73(6)	94.24(6)	100.91(6)
N-Ru-L	85.8(1)	84.48(6)	84.51(4)	I	ı	82.7(1)	74(1)	98.7(3)	84.8(2)	84.4(2)	84.9(2)
	164.9(2)	88.56(6)	85.41(4)	I	ı	84.4(2)	86(1)	177.6(3)	88.1(2)	91.0(2)	88.6(2)
S-Ru-L	87.05(6)	89.36(2)	90.96(2)	I	ı	90.6(1)	90(1)	86.5(2)	97.4(1)	91.3(1)	91.7(1)
	88.65(6)	171.77(3)	168.36(2)	ı	ı	90.8(1)	92(1)	98.2(2)	173.4(1)	175.2(1)	173.6(1)
P-Ru-L	92.56(6)	90.66(2)	94.24(2)	ı	ı	175.7(1)	178(1)	89.6(2)	92.8(1)	95.0(1)	93.6(1)

Scheme 2. Synthesis and Structures of 2-5

clearly assign aryl peaks associated with the two diastereomers, as well as the N–H proton resonances at δ 6.24 (2) and δ 5.82 (2'). Two ³¹P NMR resonances were observed at δ 45.8 (2) and δ 43.3 (2') with peak intensities similar to the diastereomeric ratio obtained from the ¹H NMR data.

Crystals of 2 suitable for single-crystal XRD were obtained by diffusion of pentane into dichloromethane solutions. The crystals revealed two visibly different morphologies, and subsequent XRD analysis revealed they were different diastereomers of Ru[H(MeSNNSMe)]Cl(PPh3) with H- $({}^{\rm Me}{\rm SNNS^{Me}})^{1-}$ bound in a cis- β arrangement (Figure 2). We were unable to assign the solid-state structures to solution NMR resonances for 2 and 2', so we have designated the XRD structures separately as 2a and 2b, respectively. Both structures indicated successful deprotonation of one H₂(MeSNNSMe) nitrogen atom. The resulting change in N hybridization (sp³ \rightarrow sp²) caused the adjacent thioanisole group to rotate into the equatorial plane so that the corresponding SMe group was oriented trans to the protonated N-H group. The two conjugated aryl groups pucker in opposite directions to give two diastereometric configurations. The deprotonated Ru-N bond distances trans to PPh₃ in both structures are significantly shorter at 2.070(2) and 2.077(2) Å compared to the protonated Ru-N distances of 2.133(2) and 2.136(2) Å, respectively. Delocalized π conjugation with the amido N atom is reflected by the N-C distances, which decrease from 1.46- 1.50 Å for sp^3 -hybridized N atoms in 1 and 2 to 1.37-1.38 Å. A defining structural metric between 2a and 2b is the P-Ru-S

angle between PPh₃ and the axial SMe group, which increased from $91.84(2)^{\circ}$ in 2b to $93.47(3)^{\circ}$ in 2a. A small but significant 0.02 Å decrease in the Ru–P distance was observed in 2a compared to that in 2b, which suggests that differences in the P–Ru–S angle may reflect subtle differences in Ru–P bonding.

Attempts to remove the second N–H proton in 2 with excess NEt₃ were unsuccessful. However, treating a benzene solution of 2 with the stronger base NaO^tBu immediately caused the yellow solution to turn dark blue. Layering the solution with pentane yielded blue crystals that were revealed to be the five-coordinate complex Ru($^{\text{Me}}$ SNNS $^{\text{Me}}$)(PPh₃) (3) by single-crystal XRD (Figure 3, left). 3 has a square pyramidal coordination geometry with *trans* ($^{\text{Me}}$ SNNS $^{\text{Me}}$)^{2–} and PPh₃. The Ru–N distances decreased from 2.143(5) and 2.173(5) Å in 1 to 2.005(6) and 2.018(6) Å in 3, and the Ru–P distance decreased by ~0.1 Å to 2.214(2) Å.

The ³¹P NMR spectrum of 3 in THF revealed a significant downfield shift at δ 89.9 relative to 1 (δ 44.5) and 2 (δ 45.8) due to the vacant coordination site trans to PPh3. A single broad resonance was observed in the 1H NMR spectrum at δ 2.53 for the two SMe groups, thereby indicating their equivalence on the NMR time scale. Only three broad peaks integrating to all 27 aryl protons (PPh3 and MeSNNSMe) were observed in the ¹H NMR spectrum. The broadened ¹H and ³¹P NMR resonances suggested that the SMe and aryl groups were rapidly adopting different configurations to give different stereoisomers of 3. Indeed, cooling solutions of 3 to -90 °C caused the room temperature (RT) ¹H NMR resonance assigned to SMe at δ 2.53 to split into a single resonance at δ 2.63 and two singlets of equal intensity at δ 2.57 and 1.87 (Figure 4). Correspondingly, the broad ³¹P NMR resonance at δ 89.9 split into two resonances at δ 85.5 and 82.8, and new aryl resonances emerged in the ¹H NMR spectrum.

We assign the single low-temperature SMe resonance at δ 2.63 to the isomer with chemically equivalent SMe groups that pointed away from PPh₃ [3 (Scheme 3)]. The two new chemically inequivalent SMe resonances at δ 2.57 and 1.87 are assigned to the stereoisomer where the SMe groups are pointed in opposite directions [3' (Scheme 3)]. Accordingly, the ³¹P NMR resonances at δ 85.5 and 82.8 are assigned to 3 and 3', respectively. We did not see clear evidence of the stereoisomer where both SMe groups point toward PPh₃ [3" (Scheme 3)], although several small unassigned resonances become more apparent in the ¹H NMR spectrum at lower temperatures

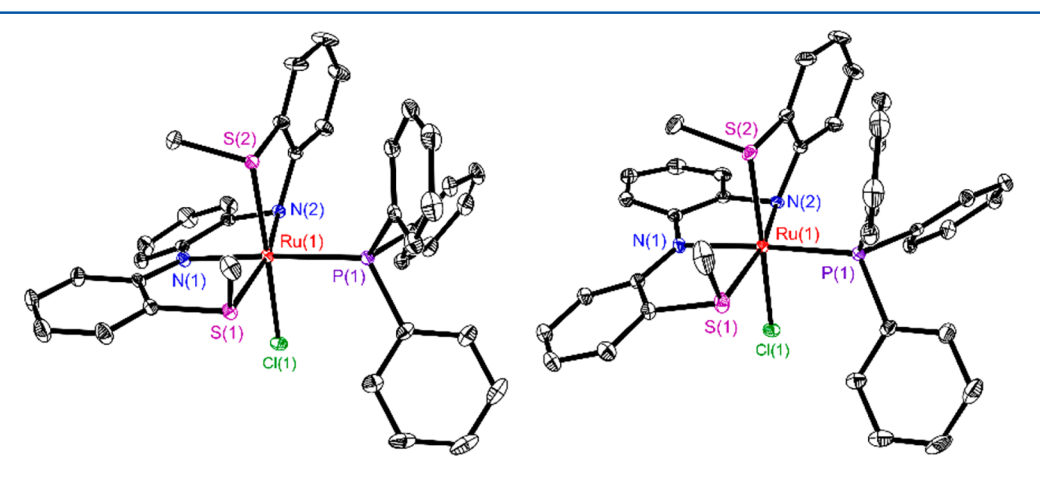


Figure 2. Molecular structures of diastereomers of 2a (left) and 2b (right). Ellipsoids are drawn at the 35% probability level. Hydrogen atoms have been omitted.

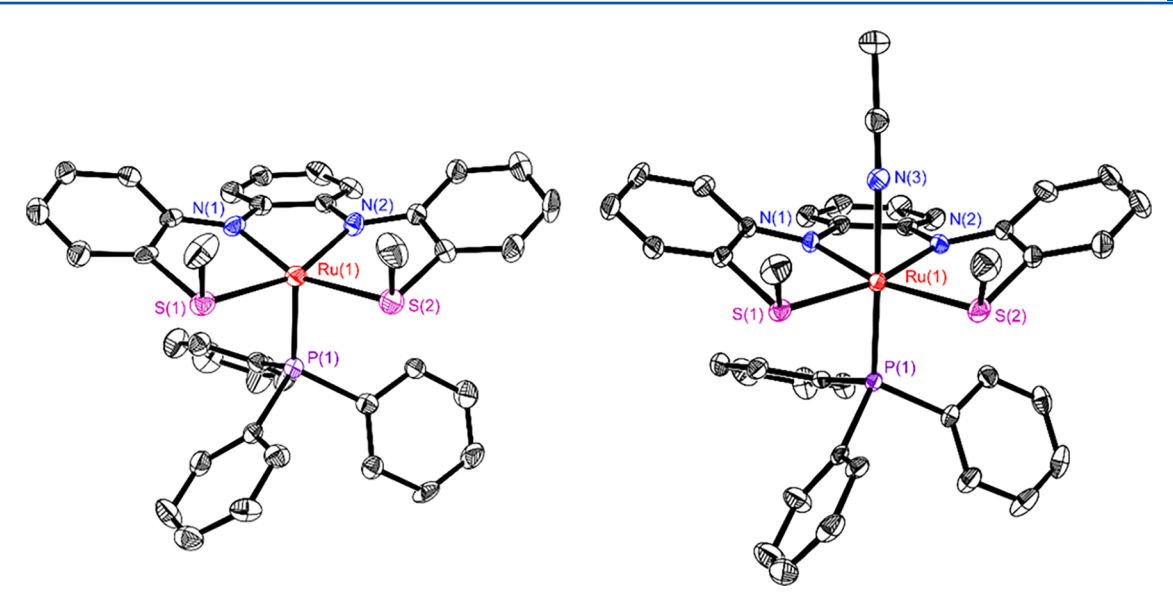


Figure 3. Molecular structures of $Ru(^{Me}SNNS^{Me})(PPh_3)$ (3, left) and $Ru(^{Me}SNNS^{Me})(PPh_3)(MeCN)$ (4, right). Ellipsoids are drawn at the 35% probability level. Co-crystallized solvent molecules and hydrogen atoms have been omitted.

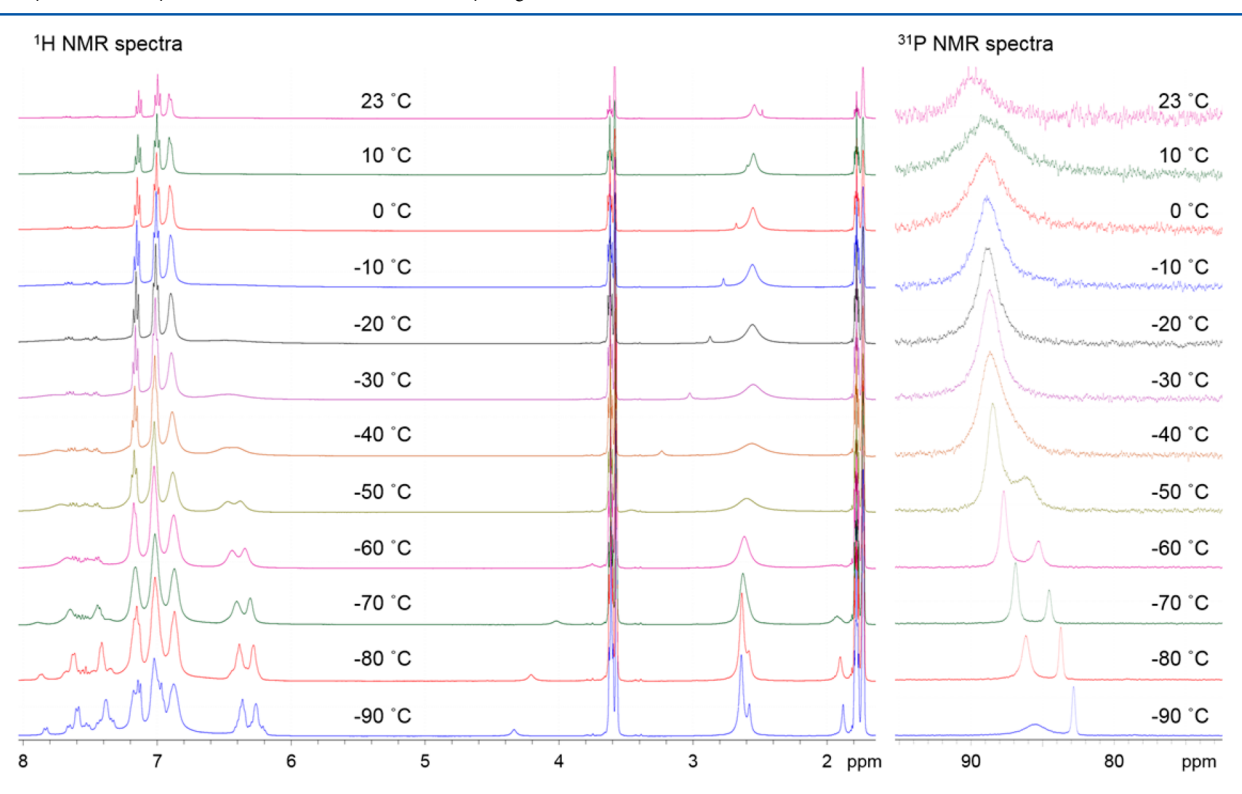


Figure 4. Variable-temperature ¹H NMR spectra (left) and ³¹P NMR spectra (right) of Ru(MeSNNSMe)(PPh₃) (3) in THF-d₈.

Scheme 3. Different Possible Orientations of the SMe Groups in 3^a

Me Me Me SPRu
$$\rightarrow$$
S Ru \rightarrow

^aThe remaining atoms on the triaryl backbone have been omitted for the sake of clarity.

(notably a resonance at δ 4.35 at -90 °C), and the line shape of the ^{31}P resonance at δ 85.5 begins to broaden again at -90 °C.

We suspect that 3" is less favored energetically over 3 and 3' because of increased degree of steric clashing with PPh₃ when both SMe groups are oriented toward PPh₃ at the same time. An alternative explanation that may also account for the different sets of NMR resonances for 3 at low temperatures is that the triaryl backbone in Ru($^{\text{Me}}$ SNNS $^{\text{Me}}$)(PPh₃) adopts different puckered orientations, as observed for the structures of 2a and 2b in Figure 2. We cannot distinguish between the two possibilities given the data at hand, but we propose the structures of 3 and 3' in Scheme 3 are more likely given the significant 1 H NMR shift difference in the SMe resonances ($\Delta\delta$ = 0.7). Overall, the variable-temperature (VT) NMR results

Organometallics Article Article

indicate dynamic exchange between at least two diastereomers in solution.

During our attempts to crystallize 3, we discovered that addition of MeCN yielded a dark solution that slowly precipitated an orange solid. Initial attempts to isolate the precipitate by filtration proved to be unproductive because the solid quickly reverted back to 3 as it evaporated to dryness; the color reverted from orange to blue, and subsequent ³¹P NMR analysis of the dissolved solid revealed only a resonance assigned to 3. However, orange crystals grown from mixtures of 3 in THF and MeCN persisted long enough for structural and spectral characterization, Single-crystal XRD studies confirmed the crystals to be Ru(MeSNNSMe)(PPh3)(MeCN) (4) with MeCN bound in the axial coordination site (Figure 3, right). Crystals of 4 were quickly isolated from the mother liquor and dissolved in C₆D₆ with addition of a small amount of MeCN to collect the NMR data. The ³¹P NMR spectrum revealed a relatively large upfield shift of δ 25.4, and the ¹H NMR spectrum revealed a single broad SMe resonance at δ 2.05 and a bound MeCN resonance at δ 0.50 (free MeCN was observed at δ 0.60, similar to that reported previously at δ 0.58). 40

Metal–Ligand Cooperativity. In the course of investigating other bases to deprotonate the remaining N–H group in $Ru[H(^{Me}SNNS^{Me})]Cl(PPh_3)$ (2), we discovered that the $(^{Me}SNNS^{Me})^{2-}$ ligand is capable of participating in metal–ligand cooperativity (MLC), a type of substrate binding that involves the metal and a nucleophilic atom on the ligand. Addition of NaBH₄ to 2 in THF resulted in a color change from yellow to orange and eventually green upon workup and extraction with Et₂O. Crystallization yielded dark green prisms from concentrated Et₂O/pentane solutions at -25 °C that revealed that the second nitrogen in 2 had indeed been deprotonated as desired, but the reaction unexpectedly led to the isolation of N-capped, borane-bridged hydride $Ru[(\mu-H)BH_2](^{Me}SNNS^{Me})(PPh_3)$ (5) (Figure 5). Langer, Gade, and

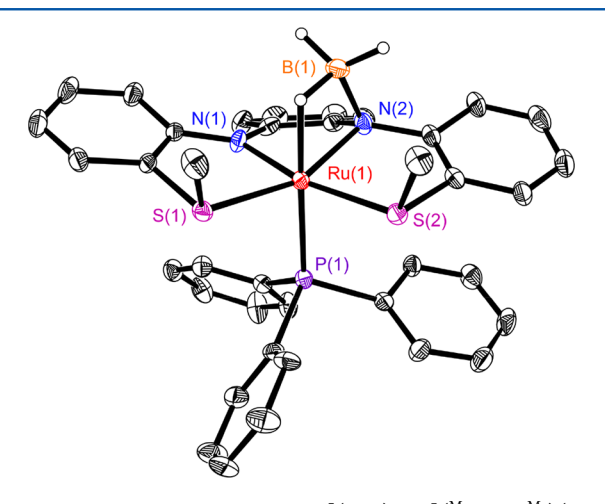


Figure 5. Molecular structures of Ru[(μ -H)BH₂](^{Me}SNNS^{Me})(PPh₃) (5). Ellipsoids are drawn at the 35% probability level. Hydrogen atoms have been omitted except for those bound to boron.

Trincado and Grützmacher separately reported this type of MLC BH3 binding across tricoordinate N-centered ligands with Fe, 41 Ru, 42 and Rh, 43 respectively. MLC binding of BH3 has also been observed across a Ru—thiolate bond involving a tetradentate S_2N_2 ligand with an ethylenediamine backbone and thiolate groups instead of thioethers. 44

Single-crystal XRD data for 5 revealed a planar ($^{\text{Me}}$ SNNS $^{\text{Me}}$) $^{2-}$ ligand and hydride *trans* to PPh₃. The B–N distance of 1.611(7) Å is similar to that observed by Gade, 1.594(3) Å. 42 The Ru–N distance for the N participating in MLC binding is longer at 2.096(4) Å, versus 2.038(4) Å. The refined BH₃ positions yielded a Ru–H distance of 1.77(4) Å. While there are well-known issues associated with accurately determining hydride locations with XRD, we note that this distance compares reasonably well to Ru–H distances reported in similar systems. Ru $^{2+}$ complexes with trialkylphosphines and a tetradentate S₂N₂ ligand with dithiolates (instead of thioethers) yielded Ru–H and Ru–H–BH₂ distances of 1.74(8) and 1.68(5) Å, respectively. Notably, the latter Ru–HBH₂ distance involved the aforementioned MLC binding with one of the thiolates on the S₂N₂ ligand.

The 11 B NMR spectrum of **5** in THF- d_8 revealed a broad resonance at δ –13.9 assigned to the MLC-bound BH₃. A broad doublet was observed in the hydride region of the 1 H NMR spectrum at δ –6.62 in C₆D₆ ($^{2}J_{PH}$ = 65 Hz). Two inequivalent SMe resonances were observed at δ 2.44 and 2.94 in a 1:1 ratio, as expected because of the asymmetry induced by capping one nitrogen. Occupation of the open coordination in **5** caused the broad singlet in the 31 P NMR spectrum of **3** at δ 89.9 to shift upfield and split into a doublet at δ 50.3 ($^{2}J_{PH}$ = 65 Hz). The terminal B–H resonances were not observed in the 1 H NMR spectrum of **5** even when the solutions were cooled to –90 °C. Difficulties observing the terminal B–H 1 H NMR resonances have been reported previously in other MLC-bound BH₃ complexes, 41,43 but the infrared (IR) spectrum of **5** confirmed their presence.

Compounds with MLC-bound BH $_3$ generally fall into one of two categories according to their IR spectra: (1) those with two absorptions assigned to terminal B–H stretching (symmetric and asymmetric) in the B–H stretching region (~2200–2500 cm $^{-1}$) and one M–H–B stretch at lower wavenumbers (~1700–2000 cm $^{-1}$) 42,44 and (2) those with three absorptions assigned to one symmetric and two asymmetric B–H stretches (i.e., no M–H–B stretch at significantly lower wavenumbers).

These two categories can been further classified as those in which there is a strong M–H interaction (case 1) or, as described by Grützmacher and co-workers, ⁴³ those in which the M–H interaction is weak (case 2). The IR data collected for 5 were consistent with the latter situation (case 2): three B–H stretches were observed at 2338, 2404, and 2430 cm⁻¹ in the solid state (Figure S26). No IR resonance that can be assigned to a Ru–H stretch was observed at a lower energy, and similar IR resonances were observed in solutions of 5 in benzene (2348, 2416, and 2455 cm⁻¹) and THF (2343, 2413, and 2454 cm⁻¹). It is important to note that the M–H–B hydride resonances, as reported above for 5, are still observed in the ¹H NMR spectra despite weak M–H bonding.⁴³

Reactivity of Ru(MeSNNSMe)(PPh₃) (3) with CO and Acids. The reversible binding of MeCN to 3 led us to investigate how increasing the field strength of the neutral donor ligand affected its affinity for the open coordination site. We postulated that stronger field ligands such as CO would bind irreversibly. Treating a benzene solution of 3 with CO resulted in an immediate change in color from blue to red, and XRD analysis of red crystals grown from pentane revealed the complex to be Ru(MeSNNSMe)(CO)(PPh₃) [6 (Scheme 4 and Figure 6)]. However, the crystal structure revealed CO bound trans to one of the amido groups and (MeSNNSMe)²⁻ distorted

Organometallics Article Article

Scheme 4. Synthesis and Structures of 6-8

$$\begin{array}{c} \text{BF}_4 \\ \text{N=Ru-PPh}_3 \\ \text{L=THF (7)} \end{array} \begin{array}{c} \text{HBF}_4 \cdot \text{Et}_2\text{O} \\ \text{THF} \\ \text{PhCO}_2\text{H} \end{array} \begin{array}{c} \text{SMe} \\ \text{Co} \\ \text{N=Ru-PPh}_3 \\ \text{N=Ru-PPh}_3 \\ \text{N=Ru-PPh}_3 \\ \text{SMe} \\ \text{L=PhCO}_2 \cdot (8) \end{array}$$

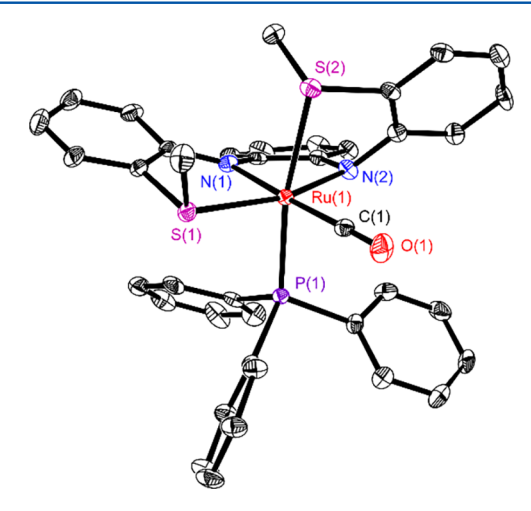


Figure 6. Molecular structure of $Ru(^{Me}SNNS^{Me})(CO)(PPh_3)$ (6). Ellipsoids are drawn at the 35% probability level. Hydrogen atoms and a co-crystallized pentane molecule have been omitted.

in a cis- β arrangement, as reflected in the P-Ru-S angles of 92.73(7)° (cis) and 169.61(7)° (trans). The Ru-S distance trans to PPh₃ increased to 2.432(2) Å relative to the cis Ru-S distance of 2.354(2) Å, and the Ru-N distance trans to CO at 2.062(5) Å was slightly shorter than the Ru-N distance trans to SMe at 2.077(6) Å. The Ru-CO distance was 1.863(7) Å, and the C-O distance was 1.152(9) Å.

 ^1H NMR data revealed the S_2N_2 ligand in 6 was no longer symmetric, corroborating the observed ligand distortion to accommodate CO binding in the equatorial position. Two SMe resonances were observed at δ 1.58 and 2.16, and the resonance corresponding to the SMe group trans to PPh3 at δ 1.58 split into a doublet due to four-bond P–H coupling ($^4J_{\rm H-P}=2.8$ Hz). The $^{31}\rm P$ NMR resonance in C_6D_6 shifts upfield from δ 89.9 in 3 to δ 44.7 in 6. Solution IR measurements collected in THF revealed a single CO stretch at 1937 cm $^{-1}$. The CO in 6 is more activated than those observed in Ru(S4)(CO)(PPh3) complexes (1963–1964 cm $^{-1}$) that have thioether groups trans to CO. 45,46

We ascribe the equatorial CO binding preference in 6 to established differences in *trans* influence among CO, amido, thioethers, and triphenylphosphine. CO is a strong π -acceptor ligand (i.e., strong field ligand), and amido groups are strong π donors (i.e., weak field ligand); on the other hand, thioethers

and phosphines lie within these two extremes. As a consequence, we suspect that the *trans* N–Ru–CO preference in **6** stems from strong Ru \rightarrow CO backbonding that stabilizes amido $\pi \rightarrow$ Ru donation, which is supported by the CO stretching comparisons to Ru complexes with *trans* thioether groups described above. As, 46 Remarkably, the bonding stabilization appears to be more than enough to offset the energy required to distort the conjugated (MeSNNSMe)²⁻ ligand.

To investigate the acid—base chemistry of the $(^{Me}SNNS^{Me})^{2-}$ ligand and evaluate the possibility of other forms of metal—ligand bifunctional reactivity across Ru—N bonds, ⁴⁷ we treated five-coordinate 3 with HBF₄·Et₂O and benzoic acid (PhCO₂H). HBF₄·Et₂O was selected to determine if we could selectively protonate one N position in the absence of a coordinating anion.

Addition of $HBF_4 \cdot Et_2O$ to a concentrated solution of 3 in THF yielded a yellow precipitate. XRD studies of yellow crystals grown from THF and pentane revealed {Ru[H-(MeSNNSMe)](PPh₃)(THF)}BF₄ [7 (Figure 7)]. The structure of 7 is similar to that of the diastereomers of Ru[H-(MeSNNSMe)](PPh₃)Cl, the key exception being that a THF molecule occupies the site *trans* to the axial SMe instead of chloride. Interestingly, the site *trans* to SMe is capable of

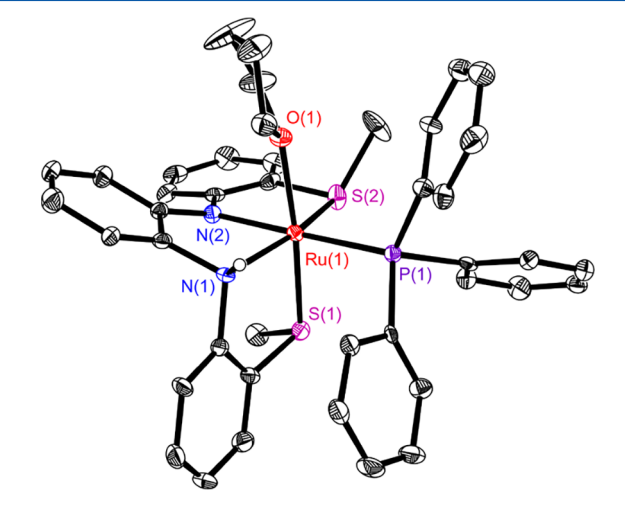


Figure 7. Molecular structure of $\{Ru[H(^{Me}SNNS^{Me})](PPh_3)(THF)\}$ -BF₄ (7). Ellipsoids are drawn at the 35% probability level. Hydrogen atoms attached to C have been omitted.

binding a THF molecule, whereas we see no evidence of binding of THF to the open coordination site *trans* to PPh₃ in 3; single crystals of 3 were isolated from concentrated THF solutions in several reactions, and ^{31}P NMR analysis of 3 in noncoordinating C_6D_6 revealed a broad chemical shift identical to that observed in THF- d_8 (δ 89.8).

Like 2, the ^1H and ^{31}P NMR spectra of 7 in THF- d_8 reveal resonances assigned to two diastereomers, but the relative abundance of the major diastereomer was much higher (\sim 6:1 for 7 vs \sim 2:1 for 2). This difference is likely attributed in part to the greater steric profile of THF in 7 compared to that of chloride in 2, thereby giving stronger preference to the diastereomer that more effectively minimizes steric interactions. The major diastereomer has SMe ^1H resonances at δ 1.76 and 1.91, whereas a smaller set of resonances is assigned to the minor diastereomer at δ 1.56 and 1.89. As expected, the ^{31}P NMR spectrum yielded two resonances assigned to the two diastereomers at δ 39.0 (major) and δ 38.1 (minor). ^{11}B and ^{19}F NMR spectra confirmed the presence of the non-coordinating BF₄ $^-$ counteranion in 7 with single resonances observed at δ –0.81 and –151.1, respectively.

Treating a solution of 3 in THF with benzoic acid formed the monoprotonated compound $Ru[H(^{Me}SNNS^{Me})](PPh_3)-(PhCO_2)$ (8) with a bound benzoate anion (Figure 8). The

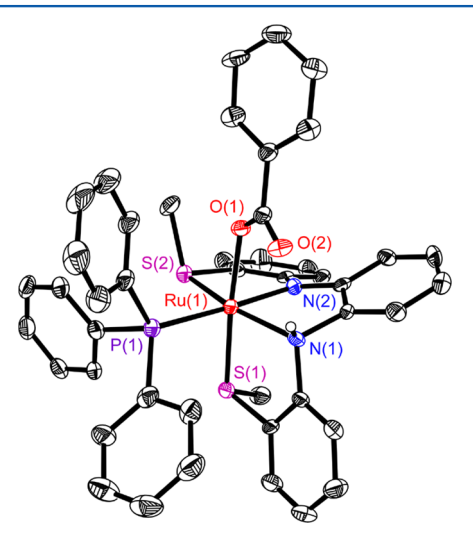


Figure 8. Molecular structure of Ru[H(^{Me}SNNS^{Me})](PPh₃)(PhCO₂) (8). Ellipsoids are drawn at the 35% probability level. Hydrogen atoms attached to C and the second molecule have been omitted.

unbound carbonyl group hydrogen bonds with the N–H proton, and the corresponding 1H NMR resonance was observed at δ 10.9 in C_6D_6 . This broad peak is shifted more downfield compared to those in 1 (δ 7.92 and 9.72), 2 (δ 6.24), 2' (δ 5.82), and 7 (δ 8.18) due to hydrogen bonding interactions with Ru-bound benzoate. Unlike those of 2 and 7, the NMR data for 8 revealed only one discernible diastereomer in solution. One set of chemically inequivalent SMe resonances was observed in the 1H NMR spectrum at δ 1.58 and 2.52, and only one ^{31}P NMR resonance was observed at δ 46.0. Two new symmetric and asymmetric C–O stretches assigned to the benzoate were observed in the IR spectrum at 1363 and 1598 cm $^{-1}$, respectively. These compare reasonably well to those reported by Leitner and co-workers 48 for [Ru(Acriphos)-(PPh₃)(Cl)(PhCO₂)] at 1327 and 1625 cm $^{-1}$, respectively.

Electrochemical Studies. To investigate the redox activity of our Ru S_2N_2 complexes, we collected the cyclic voltammogram of 3 in THF (Figure 9). We focused our preliminary

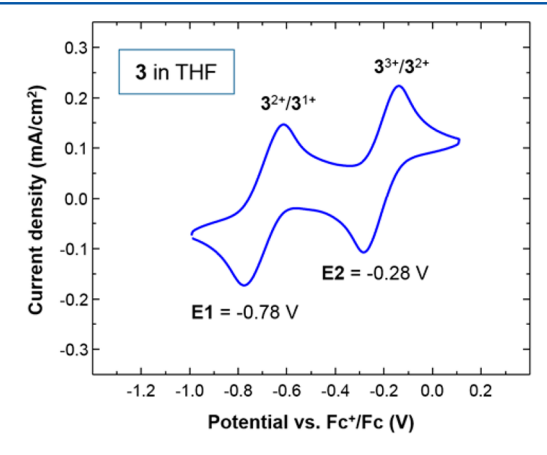


Figure 9. Cyclic voltammogram of $Ru(^{Me}SNNS^{Me})(PPh_3)$ (3) collected in THF with 0.1 M ($^{t}Bu_4N)PF_6$ and a glassy carbon working electrode (scan rate of 100 mV/s). A platinum wire was used as the counter and quasi reference electrodes.

efforts on 3 because they contain planar ($^{\text{Me}}\text{SNNS}^{\text{Me}}$)²⁻ ligands that can facilitate reversible ligand-centered electroactivity without structural rearrangement. The cyclic voltammogram of 3 in THF yielded two reversible redox waves at -0.78 and -0.28 V versus Fc⁺/Fc (E1 and E2, respectively) and an irreversible reduction wave at -2.46 V (Figure S2). Additional redox waves appear in the cyclic voltammogram when the electrochemical window is expanded to include the irreversible reduction wave at -2.46 V due to the generation of electrochemically active decomposition products.

The redox waves in the cyclic voltammogram of 3 were tentatively assigned by comparison to other Ru(II) complexes with o-phenylenediamine and o-phenylenediamine-derived ligands. In general, three redox features are typically observed, two associated with ligand-centered redox events (as shown in Chart 1) and one assigned to the Ru3+/Ru2+ redox couple at more positive potentials. For example, Mascharak and coworkers 49,50 reported two reversible redox events at -0.73 and 0.45 V versus Fc⁺/Fc and an irreversible redox event at -1.35 Vin the cyclic voltammogram of a cis- α (P₂N₂)RuCl₂ complex. They assigned the irreversible feature at -1.35 V as a ligandcentered reduction of the o-diiminosemiquinone radical to a fully reduced o-phenylenediamine unit. The reversible wave at -0.73 V was assigned to the second ligand-centered redox event, and the reversible wave at 0.45 V was assigned to the Ru³⁺/Ru²⁺ redox couple. Similar observations and assignments were reported by Goswami and co-workers for a series of Ru²⁺ complexes with aryl- and N-substituted o-phenylenediamine ligands. 10,51 Skara et al. 18 calculated reduction potentials of -2.70 V (ligand), -1.26 V (ligand), and 0.54 V (metal) versus Fc^{+}/Fc reported for $[(en)_{2}Ru(L)]^{n}$, where en = ethylenediamine and L = o-phenylenediamine, which corroborated the sequence of the assignments of Mascharak and Goswami.

On the basis of these previous reports, we tentatively assign the irreversible feature at -2.46 V as the $3^{1+}/3$ redox event corresponding to reduction of the o-diiminosemiquinone radical to the fully reduced o-phenylenediamine backbone. E1 corresponds to the second ligand redox couple and is assigned as $3^{2+}/3^{1+}$, whereas E2 is assigned as $3^{3+}/3^{2+}$ and corresponds

to the Ru³⁺/Ru²⁺ redox couple. We are currently using in situ spectroscopy, chemical reduction methods, and density functional theory calculations to confirm these assignments and to determine the structures of these electrochemically active species as they are generated. These investigations, as well as electrochemistry of 5 with MLC-bound BH₃, are currently in progress and will be described in a future report.

CONCLUSION

In summary, we described the synthesis and characterization of the triaryl S₂N₂ ligand, H₂(MeSNNSMe), and showed it can be sequentially deprotonated when bound to Ru(II). Treating Ru(MeSNNSMe)(PPh3) (3) with CO changed the trans $(^{Me}SNNS^{Me})^{2-}$ ligand arrangement to cis- β in Ru $(^{Me}SNNS^{Me})$ -(CO)(PPh₃). In contrast, MeCN binds reversibly to the open coordination site in 3 without significantly affecting the S₂N₂ ligand structure. We showed that Ru(MeSNNSMe)(PPh3) reacts with HBF4·Et2O and benzoic acid to form the octahedral complexes [Ru[H(MeSNNSMe)](PPh3)(THF)]BF4 and Ru[H-(MeSNNSMe)](PPh₃)(PhCO₂). Most notably, we demonstrated that the (MeSNNSMe)2- ligand is both redox-active and capable of participating in metal-ligand cooperativity with Ru. Cyclic voltammogram traces of square pyramidal Ru(MeSNNSMe)-(PPh₃) in THF revealed three redox events, two assigned to the ligand and one to the metal, and a deprotonated amido group in 3 participates in MLC binding of BH₃. Future work will be aimed at understanding how MLC binding is affected under an applied potential, and exploring the utility of redox-active and MLC-capable tetradentate ligands in electrocatalytically driven small molecule transformations.

EXPERIMENTAL SECTION

All reactions were performed under an atmosphere of N_2 or Ar using a glovebox or standard Schlenk techniques, unless stated otherwise. Hexane, pentane, toluene, Et₂O, THF, MeCN, and dichloromethane (DCM) were dried and degassed using a Pure Process Technologies Solvent Purification System. Benzene was dried over activated 4 Å molecular sieves and deoxygenated by freeze—pump—thaw methods. NEt₃ was distilled from KOH under N_2 prior to use. Deuterated solvents except for DMSO- d_6 were deoxygenated by three freeze—pump—thaw cycles and stored over 3 Å molecular sieves. All other chemicals were purchased from commercial vendors and used as received.

¹H and ³¹P NMR data were recorded on a Bruker AVANCE-300 instrument operating at 300 MHz for ¹H and 121.5 MHz for ³¹P or on a Bruker DRX-400 instrument operating at 400 and 162 MHz for ¹H and ³¹P, respectively. ¹H and ¹³C NMR data were collected on a Bruker AVANCE-500 instrument operating at 500 and 126 MHz for ¹H and ¹³C, respectively. ¹¹B and ¹⁹F NMR data were collected on a Bruker DRX-400 instrument operating at 128 and 376.5 MHz, respectively. Chemical shifts are reported in δ units relative to residual solvent peaks (1 H and 13 C), 85% $H_{3}PO_{4}$ (^{31}P), $BF_{3}\cdot Et_{2}O$ (^{11}B), or 0.05% $C_{6}H_{5}CF_{3}$ in $C_{6}D_{6}$ (^{19}F). Microanalytical data (CHN) were collected by Midwest Microlab LLC or using an EAI CE-440 Elemental Analyzer in the University of Iowa Department of Chemistry. IR spectra were acquired on a Thermo Scientific Nicolet iS5 instrument using an attenuated reflection accessory or on samples prepared as KBr pellets, Nujol mulls between NaCl plates, or solutions between NaCl plates. Melting points were determined in sealed capillaries using a REACH MP device. HR-ESI mass spectra were recorded on a Waters GCT Premier Instrument using TOF. Fragment ions (M, molecule; L, ligand) were assigned on the basis of comparison to calculated natural abundance isotopic distributions.

N,N'-Bis[2-(methylthio)phenyl]-1,2-diaminobenzene [H_2 (MeSNNSMe)]. Pd_2 (dba) $_3$ (0.424 g, 0.462 mmol, 5 mol % based on diamine), rac-BINAP (0.432 g, 0.69 mmol, 7.5 mol %), and NaO^tBu

(2.67 g, 27.8 mmol) were added to a dry toluene (50 mL) solution of o-phenylenediamine (1.0 g, 9.2 mmol) and 2-bromothioanisole (3.7 g, 18 mmol). The reaction mixture was heated to reflux for 14 h under N2. After cooling to RT, the mixture was treated with a saturated aqueous solution of NH₄Cl immediately upon being exposed to air. The mixture of aqueous and organic layers was filtered through a pad of Celite and washed with toluene until the filtrate was colorless. The organic phase was separated, concentrated under reduced pressure, and purified by column chromatography on 70-230 mesh silica gel (8:92 CH₂Cl₂/hexane) to afford a crystalline-white solid. Yield: 4.43 g (74%). Anal. Calcd for C₂₀H₂₀N₂S₂: C, 68.14; H, 5.72; N, 7.95. Found: C, 68.32; H, 5.90; N, 8.00. HR-MS: m/z 353.6 [M + H]⁺. ¹H NMR (500 MHz, CDCl₃): δ 2.28 (s, 6H, S-CH₃), 6.66 (br, 2H, NH), 6.83 (td, 2H, J = 1.1, 7.5, 14.8 Hz, Ar-H), 7.02 (dd, 2H, J = 0.7, 8.1 Hz, Ar-H), 7.06 (dd, 2H, J = 3.27, 5.8 Hz, Ar-H), 7.14 (td, 2H, J = 1.4, 8.2, 15.5 Hz, Ar-H), 7.33 (dd, 2H, J = 3.4, 5.8 Hz, Ar-H), 7.44 (dd, 2H, J = 1.4, 7.7 Hz, Ar-H). 13 C NMR (126 MHz, CDCl₃): δ 18.14, 114.89, 120.33, 121.72, 123.74, 123.77, 128.79, 133.46, 135.00, 144.42. IR (cm⁻¹): 3361 m, 3328 m, 2780 w, 1581 m, 1574 m, 1518 m, 1461 s, 1416 w, 1377 s, 1324 m, 1301 m, 1275 w, 1216 w, 1158 w, 1130 w, 1101 w, 1067 m, 1036 m, 968 w, 899 w.

{Ru[H₂(MeSNNSMe)]Cl(PPh₃)}Cl (1). A 100 mL Schlenk tube was charged with RuCl₂(PPh₃)₃ (0.55 g, 0.57 mmol), H₂(MeSNNSMe) (0.20 g, 0.57 mmol), and THF (20 mL). The reaction mixture was heated to reflux overnight, which precipitated a yellow solid. After cooling to RT, the precipitate was filtered, washed with Et₂O (20 mL), and evaporated to dryness under vacuum. The solid was dissolved in CH₂Cl₂, filtered over Celite, and layered with pentane to yield yellow blocks after 3 or 4 days. Yield: 0.19 g (42%). Anal. Calcd for C₃₈H₃₅N₂S₂Ru₁Cl₂P₁: C, 58.01; H, 4.48; N, 3.56. Found: C, 58.38; H, 4.67; N, 3.32. HR-MS: m/z 751.06 [M]⁺. ¹H NMR (400 MHz, DMSO- d_6): δ 2.05 (s, 3H, S-CH₃), 2.37 (s, 3H, S-CH₃), 7.08 (m, 2H, Ar-H), 7.23 (d, 1H, I = 8.1 Hz, Ar-H), 7.29–7.43 (m, 20H, Ar-H), 7.59 (vt, 1H, Ar-H), 7.79 (dd, 1H, J = 1.2 Hz, 7.8 Hz, Ar-H), 7.88 (d, 1H, J = 8.2 Hz, Ar-H), 7.93 (br, 1H, N-H), 8.42 (d, 1H, J = 8.1 Hz, Ar-H), 9.72 (br, 1H, N-H). $^{31}P\{^{1}H\}$ NMR (121.5 MHz, DMSO- d_6): δ 44.5 (s). IR (cm⁻¹): 3363 br, 3123 m, 2727 m, 2688 w, 1578 w, 1305 s, 1264 m, 1183 w, 1157 br, 1104 w, 1090 s, 1071 m, 1039 m, 999 m, 961 s, 891 m, 856 m, 821 s, 775 s, 740 s, 722 s, 698 s, 682 s, 614 s, 578

 $Ru[H(^{Me}SNNS^{Me})]Cl(PPh_3)$ (2). $RuCl_2(PPh_3)_3$ (1.09 g, 1.14 mmol) and $H_2(^{Me}SNNS^{Me})$ (0.40 g, 1.1 mmol) were added to a 20 mL scintillation vial, followed by benzene (15 mL) and NEt₃ (160 μ L, 1.14 mmol). The reaction mixture was stirred for 12 h at RT to afford a yellow precipitate. The precipitate was filtered, washed with Et₂O (50 mL), and evaporated to dryness under vacuum. The precipitate was dissolved in CH2Cl2, filtered, and layered with pentane to afford yellow prisms after 4 days. Yield: 0.55 g (64%). Mp: 192 °C. Anal. Calcd for C₃₈H₃₄N₂S₂Ru₁Cl₁P₁: C, 60.83; H, 4.57; N, 3.73. Found: C, 60.11; H, 4.50; N, 3.55. ¹H NMR (400 MHz, CD₂Cl₂, -80 °C): δ 1.53 (s, SMe, 2', 3H), 1.72 (s, SMe, 2, 3H), 1.86 (s, SMe, 2, 3H), 2.51 (s, SMe, 2', 3H), 5.82 (s, NH, 2', 1H), 6.24 (s, NH, 2, 1H), 6.38 (t, *J* = 7.6 Hz, 2), 6.49 (t, J = 7.4 Hz, 2'), 6.56 (t, J = 7.6 Hz, 2), 6.66 (d, J = 7.9 Hz, 2), 6.76 (d, J = 7.9 Hz, 2'), 6.90 - 7.10 (m), 7.16 (m), 7.20 - 7.39 (m), 7.45(m), 7.63 (d, J = 8.2 Hz, 2'), 7.71 (d, J = 8.2 Hz, 2'), 7.76 (d, J = 8.4Hz, 2). ³¹P NMR (121.5 MHz, CD₂Cl₂, 20 °C): δ 43.3 (s, 2') and 45.8 (s, 2). ³¹P NMR (121.5 MHz, CD_2Cl_2 , -80 °C): δ 46.0 (s, 2') and 47.0 (s, 2). Ru(MeSNNSMe)(PPh₃) (3). NaO^tBu (0.030 g, 0.31 mmol) was

Ru(^{Me}SNNS^{Me})(**PPh**₃) (3). NaO^tBu (0.030 g, 0.31 mmol) was added to a 20 mL scintillation vial containing 2 (0.20 g, 0.26 mmol) in benzene (15 mL). The yellow solution immediately turned dark blue. The mixture was stirred for 30 min at RT and filtered through a plug of silica gel, and the solution was concentrated and layered with pentane to afford dark blue crystals. Yield: 0.11 g (59%). Anal. Calcd for $C_{38}H_{33}N_2S_2Ru_1P_1$: C, 63.94; H, 4.66; N, 3.92. Found: C, 63.90; H, 4.73; N, 3.80. Mp: 195 °C. ¹H NMR (400 MHz, THF- d_8 , 20 °C): δ 2.53 (br s, SMe), 6.91 (d, J = 6.1 Hz), 6.99 (t, J = 7.2 Hz), 7.13 (t, J = 7.2 Hz), 7.44 (m), 7.51 (m), 7.67 (m). ¹H NMR (400 MHz, THF- d_8 , -90 °C): δ 1.87 (s, SMe, 3'), 2.57 (s, SMe, 3'), 2.63 (s, SMe, 3), 6.26 (br m), 6.35 (br m), 6.78 (br s), 7.02 (br m), 7.13 (br m), 7.37 (br m),

Organometallics Article Article

7.59 (br m), 7.82 (br d). $^{31}\mathrm{P}$ NMR (162 MHz, THF- d_8 , 20 °C): δ 89.9 (br s). $^{31}\mathrm{P}$ NMR (162 MHz, THF- d_8 , -90 °C): δ 82.8 (s), 85.5 (br s). IR (ATR, cm $^{-1}$): 3048 m, 2972 w, 2913 m, 2859 w, 1577 s, 1563 s, 1545 sh, 1451 vs, 1479 w, 1469 w, 1447 vs, 1321 vs, 1310 m, 1303 m, 1291 m, 1262 w, 1241 m, 1226 m, 1204 m, 1186 m, 1154 w, 1147 w, 1122 w, 1093 m, 1087 m, 1063 m, 1057 m, 1032 m, 997 w, 972 w, 957 w, 941 m, 916 m, 909 sh, 886 m, 861 w, 850 w, 843 sh, 824 m, 751 sh, 741 s, 732 s, 719 s, 699 sh, 691 vs, 661 m.

Ru(MeSNNSMe)(NCCH₃)(PPh₃) (4). Acetonitrile (0.015 g, 0.29 mmol, 17 μ L) was added to a solution of 3 (0.20 g, 0.28 mmol) in THF (10 mL) at RT. Storing the solution at -25 °C yielded orange crystals. Yield: 90 mg (43%). ¹H NMR (400 MHz, C₆D₆): δ 7.77 (m, 2H, Ar-H), 7.74 (m, 2H, Ar-H), 7.21-7.13 (m, 6H, PPh₃), 7.06-6.96 (m, 8H, Ar-H), 6.87 (m, 9H, PPh₃), 2.05 (6H, br, S-CH₃), 0.50 (s, 3H, CH₃CN). ³¹P NMR (121.5 MHz, C₆D₆): δ 25.4 (s). Satisfactory EA data could not be obtained because of the rapid loss of coordinated MeCN upon isolation.

 $Ru[(\mu - H)BH_2](^{Me}SNNS^{Me})(PPh_3)$ (5). A solution of NaBH₄ (10 mg, 0.26 mmol) in THF (10 mL) was added to a solution of 2 (0.10 g, 0.13 mmol) in THF (15 mL). The mixture was stirred at room temperature for 12 h, and the color of the greenish-yellow solution turned orange. The reaction mixture was evaporated to dryness under vacuum. The solid residue was extracted with Et₂O (13 mL), resulting in a dark green solution that was filtered through a pad of Celite. The crude product was recrystallized from Et₂O/pentane at -25 °C to yield dark green crystals. Yield: 60 mg (63%). Mp: 162 °C. Anal. Calcd for C₃₈H₃₆B₁N₂S₂Ru₁P₁: C, 62.72; H, 4.99; N, 3.85. Found: C, 62.56; H, 5.22; N, 3.64. HR-MS: m/z 728.18 [M + H]⁺, 714.09 [M – BH₃]⁺. ¹H NMR (300 MHz, C_6D_6): δ –6.28 (br d, 1H, J = 60 Hz, Ru-H-B), 2.07 (s, 3H, S-CH₃), 2.55 (s, 3H, S-CH₃), 6.41 (m, 2H, Ar-H), 6.57 (m, 3H, Ar-H), 6.81–6.92 (m, 9H, PPh₃), 6.96–7.04 (m, 2H, Ar-H), 7.22 (t, 6H, J = 8.2 Hz, PPh₃), 7.58 (d, J = 8.1 Hz, Ar-H), 7.77 (d, J =8.1 Hz, Ar-H), 7.95 (d, I = 8.1 Hz, Ar-H). ¹¹B{¹H} NMR (128 MHz, C_6D_6): $\delta -12.2$ (br s). ³¹P{¹H} NMR (121.5 MHz, C_6D_6): δ 51.1 (s). IR (ATR, cm⁻¹): 3047 m, 2970 w, 2848 w, 2430 m, 2404 s, 2338 m, 1576 w, 1563 s, 1545 sh, 1473 s, 1456 vs, 1432 vs, 1356 vs, 1293 m, 1245 w, 1226 m, 1212 w, 1183 s, 1167 w, 1161 w, 1149 m, 1122 w, 1109 w, 1092 m, 1062 m, 1026 m, 981 s, 940 m, 898 m, 762 s, 741 m, 733 s, 695 vs, 639 m, 620 m, 602 s, 593 m, 578 s, 567 vs, 557 m. Selected IR (C₆H₆, cm⁻¹): 2348 m, 2416 s, 2455 s. Selected IR (THF, cm⁻¹): 2343 m, 2413 s, 2454 s.

Alternative Synthesis of 5. To a solution of 3 (0.10 g, 0.14 mmol) in THF (20 mL) was added 1 M THF·BH₃ in THF (100 μ L, 0.1 mmol) at RT. The dark blue solution instantly turned dark green and was allowed to stir for ~30 min before the solvent was removed under vacuum. The dark green residue was extracted with Et₂O (20 mL) and filtered through a pad of Celite. Green crystals were obtained by cooling concentrated Et₂O/pentane or THF solutions to -25 °C. 1 H, 31 P, and 11 B NMR data collected on the green crystals matched those reported above for 5.

Ru(MeSNNSMe)(CO)(PPh3) (6). A 50 mL Schlenk tube containing a blue solution of 3 (0.20 g, 0.28 mmol) in C₆H₆ (20 mL) was subjected to one freeze-pump-thaw cycle and then backfilled with 1 atm of CO gas at RT. The solution immediately turned red. The solution was stirred for 10 min, evaporated to dryness under vacuum, and extracted with Et₂O (40 mL). The solution was filtered through Celite, evaporated to dryness under vacuum, and recrystallized from pentane to afford 6 as a red crystalline solid. Yield: 185 mg (89%). Anal. Calcd for C₃₉H₃₃N₂OPRuS₂·C₅H₁₂: C, 64.92; H, 5.57; N, 3.44. Found: C, 64.56; H, 5.36; N, 3.60. Mp: 250 °C. ¹H NMR (400 MHz, C₆D₆): δ 1.58 (d, 3H, J = 2.8 Hz, S-CH₃), 2.16 (br, 3H, S-CH₃), 6.33 (td, 1H, J = 0.8, 6.8, 13.6 Hz, Ar-H), 6.47 (td, 1H, J = 1.6, 6.8, 13.6 Hz, Ar-H),6.56 (td, 1H, J = 1.6, 6.0, 13.6 Hz, Ar-H), 6.66 (td, 1H, J = 1.2, 6.4, 13.6 Hz, Ar-H), 6.77 (dd, 1H, *J* = 1.2, 6.4 Hz, Ar-H), 6.96 (m, 11H, Ar-H), 7.19-7.17 (m, 1H, Ar-H), 7.31 (ddd, 2H, J = 1.2, 2.4, 10.4 Hz, Ar-H), 7.56 (tt, 6H, J = 2.4, 7.2 Hz, Ar-H), 7.65 (td, 2H, J = 1.2, 6.8, 18.8 Hz, Ar-H). ³¹P NMR (121.5 MHz, C_6D_6): δ 44.7 (s). IR (ATR, cm⁻¹): 2964 s, 2917 vs, 2848 vs, 1931 vs (C \equiv O), 1922 vs (C \equiv O), 1738 vs, 1582 w, 1557 w, 1473 vs, 1462 vs, 1430 vs, 1372 br, 1340 s, 1277 w, 1238 vs, 1203 w, 1156 m, 1117 w, 1090 s, 1026 s, 954 m, 760

m, 729 vs, 719 vs, 704 m, 691 s. Selected IR (THF, cm $^{-1}$): 1937 vs (C \equiv O).

[Ru[H(MeSNNSMe)](PPh₃)(THF)]BF₄ (7). HBF₄·Et₂O (0.068 g, 0.42 mmol, 60 μ L) was added via syringe to a solution of 3 (0.30 g, 0.42 mmol) in THF (10 mL) at RT. The reaction mixture was stirred overnight at RT, which yielded a yellow precipitate. The precipitate was filtered, washed with Et₂O (50 mL), and evaporated to dryness under vacuum. Yellow prisms were obtained after 2 days upon layering a THF solution with pentane. Yield: 240 mg (71%). Anal. Calcd for C₄₂H₄₂N₂OS₂P₁Ru₁BF₄: C, 57.73; H, 4.84; N, 3.21. Found: C, 57.65; H, 4.76; N, 3.28. HR-MS: m/z 714.09 [M – THF – BF₄ – H]⁺. Mp: 110 °C. ¹H NMR (400 MHz, THF- d_8): δ 1.76 (s, 3H, S-CH₃), 1.91 (br s, 3H, S-CH₃), 6.54 (t, 1H, J = 7.5 Hz, Ar-H), 6.63 (t, 1H, J = 7.5Hz, Ar-H), 6.93 (t, 1H, J = 7.5 Hz, Ar-H), 7.06 (t, 1H, J = 7.5 Hz, Ar-H), 7.14 (vt, 1H, J = 7.6 Hz, Ar-H), 7.25 (m, 3H, Ar-H), 7.34-7.47(m, 15H, PPh₃), 7.75 (d, 1H, J = 8.2 Hz, Ar-H), 7.82 (d, 1H, J = 8.3Hz, Ar-H), 8.08 (d, 1H, I = 8.3 Hz, Ar-H), 8.18 (br s, 1H, N-H), 8.21 (d, 1H, J = 8.3 Hz, Ar-H). Smaller S-CH₃ ¹H NMR resonances assigned to a second diastereomer were observed at δ 1.56 and 1.89, but the associated aryl resonances could not be discerned. $^{31}\mbox{P}$ NMR (162 MHz, THF- d_8): δ 39.0 (br s, major), 38.1 (br s, minor). ¹¹B NMR (128 MHz, THF- d_8): δ –0.81 (s). ¹⁹F NMR (376.5 MHz, THF d_8): δ –151.1 (br s). IR peaks (cm⁻¹): 3235 w (N-H), 2965 m, 1597 w, 1573 s, 1487 s, 1461 vs, 1433 vs, 1413 w, 1384 w, 1339 vs, 1305 w, 1287 m, 1217 w, 1089 vs, 1066 vs, 1032 m, 1007 m, 994 m, 974 m, 951 m, 907 m, 865 m, 743 vs, 722 w, 695 vs.

Ru[H(MeSNNSMe)](PPh3)(PhCO2) (8). A solution of benzoic acid (0.017 g, 0.14 mmol) in THF (3 mL) was added to a solution of 3 (0.10 g, 0.14 mmol) in THF (5 mL). The mixture was stirred at room temperature for several hours, and the color of the blue solution turned to greenish-yellow. The reaction mixture was filtered through a pad of Celite, layered with pentane, and stored at -25 °C to yield yellow crystals. Yield: 50 mg (40%). Mp: 210 °C. Anal. Calcd for C₄₅H₃₉N₂S₂Ru₁P₁O₂: C, 64.65; H, 4.70; N, 3.35. Found: C, 64.62; H, 4.77; N, 3.47. HR-MS: m/z 835.11 [M – H]⁺. ¹H NMR (300 MHz, C_6D_6): δ 1.59 (s, 3H, S-CH₃), 2.53 (br s, 3H, S-CH₃), 6.30 (t, 1H, J =7.5 Hz, Ar-H), 6.42-6.45 (m, 2H, Ar-H), 6.52-6.56 (m, 2H, Ar-H), 6.73 (t, 1H, I = 7.5 Hz, Ar-H), 6.86-6.90 (m, 3H, Ar-H), 6.93-6.97(m, 6H, Ar-H), 7.01-7.05 (m, 4H, Ar-H), 7.23 (d, 1H, J = 8.9 Hz, Ar-H), 7.37 (d, 1H, J = 8.0 Hz, Ar-H), 7.46 (d, 1H, J = 7.5 Hz, Ar-H), 7.77 (m, 8H, PPh₃), 7.93 (m, 2H, Ar-H), 10.90 (br s, 1H, N-H). $^{31}P\{^{1}H\}$ NMR (121.5 MHz, C_6D_6): δ 46.1 (s).

Single-Crystal X-ray Diffraction Studies. Single crystals obtained from CH₂Cl₂/hexane [H₂(^{Me}SNNS^{Me})], CH₂Cl₂/pentane (1, 2a, and 2b), benzene/pentane (3), THF/MeCN (4), Et₂O/pentane (5), pentane (6), or THF/pentane (7 and 8) were mounted on a MiTeGen micromount with ParatoneN oil. The data were collected as described previously. ⁵² The structures were determined with Direct Methods (SHELXT or SHELXS), and least-squares refinement (SHELXL) confirmed the location of the non-hydrogen atoms. ⁵³ All hydrogen atom positions were idealized and were allowed to ride on the attached carbon, nitrogen, or boron atoms. Anisotropic temperature factors for all non-hydrogen atoms were included in the last refinement. Structure solution and refinement were performed with Olex2. ⁵⁴ A solvent mask was applied to the refinements of 5, 7, and 8 to account for disordered solvent in the crystal lattice that could not be modeled satisfactorily. Publication figures were generated with SHELXP. ⁵³ The data collection and refinement details are provided in Tables S1 and S2.

Electrochemical Studies. Cyclic voltammetry experiments were performed under a N_2 atmosphere in a Genesis glovebox utilizing a CH Instruments CHI660D potentiostat. The electrochemical cell was purged in the glovebox for 45 min with ultra-high-purity (UHP) Ar (99.999%) before each cyclic voltammetry (CV) experiment was performed. The electrolyte was 0.1 M (1 Bu₄N)PF₆ (Aldrich, \geq 99.0%) in THF with an analyte concentration of 1 mM. The electrochemical cell consisted of a glassy carbon working electrode with a platinum wire used as the counter and quasi reference electrodes. All potentials are reported versus the Fc⁺/Fc redox couple, measured by adding a small amount (\sim 0.005 M) of ferrocene to the electrochemical

solutions at the end of each series of measurements. The electrochemical analyses included CV performed at scan rates of 10, 25, 50, 100, 200, and 300 mV/s to monitor scan rate dependence (Figure S3).

ASSOCIATED CONTENT

S Supporting Information

The Supporting Information is available free of charge on the ACS Publications website at DOI: 10.1021/acs.organomet.7b00623.

Tabulated crystallographic data, molecular structure of $H_2(^{Me}SNNS^{Me})$, NMR spectra, and IR spectra of 3 and 5 (PDF)

Accession Codes

CCDC 1568709–1568717 and 1569006 contain the supplementary crystallographic data for this paper. These data can be obtained free of charge via www.ccdc.cam.ac.uk/data_request/cif, or by emailing data_request@ccdc.cam.ac.uk, or by contacting The Cambridge Crystallographic Data Centre, 12 Union Road, Cambridge CB2 1EZ, UK; fax: +44 1223 336033.

AUTHOR INFORMATION

Corresponding Authors

*E-mail: scott-daly@uiowa.edu. *E-mail: scott-k-shaw@uiowa.edu.

ORCID ©

Scott K. Shaw: 0000-0003-3767-3236 Scott R. Daly: 0000-0001-6229-0822

Notes

The authors declare no competing financial interest.

ACKNOWLEDGMENTS

This work was generously supported by Iowa start-up funds and funding from the American Chemical Society Petroleum Research Fund (55279-DNI5) and the National Science Foundation (1650894 and 1651381). We thank Dale Swenson for collecting single-crystal XRD data.

■ REFERENCES

- (1) Broere, D. L. J.; Plessius, R.; van der Vlugt, J. I. Chem. Soc. Rev. **2015**, 44, 6886–6915.
- (2) Lyaskovskyy, V.; de Bruin, B. ACS Catal. 2012, 2, 270-279.
- (3) Boyer, J. L.; Rochford, J.; Tsai, M.-K.; Muckerman, J. T.; Fujita, E. Coord. Chem. Rev. **2010**, 254, 309–330.
- (4) Blackmore, K. J.; Lal, N.; Ziller, J. W.; Heyduk, A. F. Eur. J. Inorg. Chem. 2009, 2009, 735–743.
- (5) Berben, L. A. Chem. Eur. J. 2015, 21, 2734-2742.
- (6) Chirik, P. J. Acc. Chem. Res. 2015, 48, 1687-1695.
- (7) Blanchard, S.; Derat, E.; Desage-El Murr, M.; Fensterbank, L.; Malacria, M.; Mouries-Mansuy, V. Eur. J. Inorg. Chem. 2012, 2012, 376–389.
- (8) Balch, A. L.; Holm, R. H. J. Am. Chem. Soc. 1966, 88, 5201-5209.
- (9) Masui, H.; Lever, A. B. P.; Auburn, P. R. Inorg. Chem. 1991, 30, 2402–2410.
- (10) Mitra, K. N.; Choudhury, S.; Castineiras, A.; Goswami, S. J. Chem. Soc., Dalton Trans. 1998, 2901–2906.
- (11) Juestel, T.; Bendix, J.; Metzler-Nolte, N.; Weyhermueller, T.; Nuber, B.; Wieghardt, K. *Inorg. Chem.* **1998**, *37*, 35–43.
- (12) Khusniyarov, M. M.; Weyhermueller, T.; Bill, E.; Wieghardt, K. J. Am. Chem. Soc. 2009, 131, 1208–1221.
- (13) Khusniyarov, M. M.; Weyhermüller, T.; Bill, E.; Wieghardt, K. Angew. Chem., Int. Ed. 2008, 47, 1228–1231.
- (14) Khusniyarov, M. M.; Bill, E.; Weyhermueller, T.; Bothe, E.; Harms, K.; Sundermeyer, J.; Wieghardt, K. Chem. Eur. J. 2008, 14, 7608–7622.

(15) Chlopek, K.; Bothe, E.; Neese, F.; Weyhermueller, T.; Wieghardt, K. Inorg. Chem. 2006, 45, 6298-6307.

- (16) Skara, G.; Gimferrer, M.; De Proft, F.; Salvador, P.; Pinter, B. Inorg. Chem. 2016, 55, 2185–2199.
- (17) van der Meer, M.; Manck, S.; Sobottka, S.; Plebst, S.; Sarkar, B. Organometallics 2015, 34, 5393–5400.
- (18) Skara, G.; Pinter, B.; Geerlings, P.; De Proft, F. Chem. Sci. 2015, 6, 4109-4117.
- (19) Das, A.; Ghosh, P.; Plebst, S.; Schwederski, B.; Mobin, S. M.; Kaim, W.; Lahiri, G. K. *Inorg. Chem.* **2015**, *54*, 3376–3386.
- (20) Janes, T.; Rawson, J. M.; Song, D. Dalton Trans. 2013, 42, 10640-10648.
- (21) Ray, K.; Petrenko, T.; Wieghardt, K.; Neese, F. Dalton Trans. 2007, 1552–1566.
- (22) Herebian, D.; Bothe, E.; Neese, F.; Weyhermueller, T.; Wieghardt, K. J. Am. Chem. Soc. **2003**, 125, 9116–9128.
- (23) Ciccione, J.; Leconte, N.; Luneau, D.; Philouze, C.; Thomas, F. *Inorg. Chem.* **2016**, *55*, 649–665.
- (24) Chaudhuri, P.; Hess, M.; Mueller, J.; Hildenbrand, K.; Bill, E.; Weyhermueller, T.; Wieghardt, K. J. Am. Chem. Soc. 1999, 121, 9599–9610
- (25) Hanninen, M. M.; Paturi, P.; Tuononen, H. M.; Sillanpaa, R.; Lehtonen, A. *Inorg. Chem.* **2013**, *52*, 5714–5721.
- (26) Blackmore, K. J.; Lal, N.; Ziller, J. W.; Heyduk, A. F. *J. Am. Chem. Soc.* **2008**, 130, 2728–2729.
- (27) Ghosh, P.; Mandal, S.; Chatterjee, I.; Mondal, T. K.; Goswami, S. *Inorg. Chem.* **2015**, *54*, 6235–6244.
- (28) Patchett, R.; Magpantay, I.; Saudan, L.; Schotes, C.; Mezzetti, A.; Santoro, F. *Angew. Chem., Int. Ed.* **2013**, *52*, 10352–10355.
- (29) Mezzetti, A. Dalton Trans. 2010, 39, 7851-7869.
- (30) Khusnutdinova, J. R.; Milstein, D. Angew. Chem., Int. Ed. 2015, 54, 12236–12273.
- (31) Zhang, Y.; MacIntosh, A. D.; Wong, J. L.; Bielinski, E. A.; Williard, P. G.; Mercado, B. Q.; Hazari, N.; Bernskoetter, W. H. *Chem. Sci.* **2015**, *6*, 4291–4299.
- (32) Filonenko, G. A.; Smykowski, D.; Szyja, B. M.; Li, G.; Szczygiel, J.; Hensen, E. J. M.; Pidko, E. A. ACS Catal. 2015, 5, 1145–1154.
- (33) Chakraborty, S.; Blacque, O.; Berke, H. Dalton Trans. 2015, 44, 6560-6570.
- (34) Vogt, M.; Nerush, A.; Diskin-Posner, Y.; Ben-David, Y.; Milstein, D. Chem. Sci. 2014, 5, 2043–2051.
- (35) Huff, C. A.; Sanford, M. S. ACS Catal. 2013, 3, 2412–2416.
- (36) Huff, C. A.; Kampf, J. W.; Sanford, M. S. Organometallics 2012, 31, 4643–4645.
- (37) Sellmann, D.; Utz, J.; Heinemann, F. W. *Inorg. Chem.* **1999**, 38, 5314–5322.
- (38) Dub, P. A.; Scott, B. L.; Gordon, J. C. Organometallics **2015**, 34,
- (39) Sellmann, D.; Utz, J.; Heinemann, F. W. Inorg. Chem. 1999, 38,
- (40) Fulmer, G. R.; Miller, A. J. M.; Sherden, N. H.; Gottlieb, H. E.; Nudelman, A.; Stoltz, B. M.; Bercaw, J. E.; Goldberg, K. I. *Organometallics* **2010**, *29*, 2176–2179.
- (41) Schneck, F.; Assmann, M.; Balmer, M.; Harms, K.; Langer, R. Organometallics 2016, 35, 1931–1943.
- (42) Xu, Y.; Rettenmeier, C. A.; Plundrich, G. T.; Wadepohl, H.; Enders, M.; Gade, L. H. Organometallics 2015, 34, 5113-5118.
- (43) Muller, F.; Trincado, M.; Pribanic, B.; Vogt, M.; Grützmacher, H. J. Organomet. Chem. 2016, 821, 154–162.
- (44) Sellmann, D.; Hille, A.; Heinemann, F. W.; Moll, M.; Reiher, M.; Hess, B. A.; Bauer, W. Chem. Eur. J. 2004, 10, 4214-4224.
- (45) Sellmann, D.; Bail, P.; Knoch, F.; Moll, M. Chem. Ber. 1995, 128, 653–663.
- (46) Sellmann, D.; Engl, K.; Gottschalk-Gaudig, T.; Heinemann, F. W. Eur. J. Inorg. Chem. 1999, 1999, 333-339.
- (47) Dub, P. A.; Gordon, J. C. Dalton Trans. 2016, 45, 6756-6781.
- (48) Rohmann, K.; Kothe, J.; Haenel, M. W.; Englert, U.; Hölscher, M.; Leitner, W. Angew. Chem., Int. Ed. 2016, 55, 8966-8969.

(49) Fry, N. L.; Rose, M. J.; Nyitray, C.; Mascharak, P. K. Inorg. Chem. 2008, 47, 11604–11610.

- (50) Mascharak and co-workers reported their reduction potentials versus SCE in DMF, so a shift of -0.45 V was applied to reference them to Fc $^+$ /Fc for comparison to our values. The -0.45 V SCE to Fc $^+$ /Fc shift in DMF was obtained from: Connelly, N. G.; Geiger, W. E. *Chem. Rev.* **1996**, *96*, 877-910.
- (51) Majumdar, P.; Falvello, L. R.; Tomas, M.; Goswami, S. Chem. Eur. J. 2001, 7, 5222-5228.
- (52) Lee, K.; Wei, H.; Blake, A. V.; Donahue, C. M.; Keith, J. M.; Daly, S. R. Dalton Trans. **2016**, 45, 9774–9785.
- (53) Sheldrick, G. M. Acta Crystallogr., Sect. A: Found. Crystallogr. 2008, 64, 112–122.
- (54) Dolomanov, O. V.; Bourhis, L. J.; Gildea, R. J.; Howard, J. A. K.; Puschmann, H. *J. Appl. Crystallogr.* **2009**, *42*, 339–341.